Title

High contrast cartilaginous endplate imaging using a 3D adiabatic inversion-recovery-prepared fat-saturated ultrashort echo time (3D IR-FS-UTE) sequence

Journal

NMR in Biomedicine, 34(10)

ISSN

0952-3480

Authors

Lombardi, Alecio F
Wei, Zhao
Wong, Jonathan
et al.

Publication Date

2021-10-01

DOI

10.1002/nbm.4579

Peer reviewed

HHS Public Access

Author manuscript

NMR Biomed. Author manuscript; available in PMC 2022 March 24.

Published in final edited form as:

NMR Biomed. 2021 October ; 34(10): e4579. doi:10.1002/nbm.4579.

High Contrast Cartilaginous Endplate Imaging Using a 3D Adiabatic Inversion Recovery Prepared Fat Saturated Ultrashort Echo Time (3D IR-FS-UTE) Sequence

Alecio F. Lombardi[1,2], **Zhao Wei**[1], **Jonathan Wong**[1,2], **Michael Carl**[3], **Roland R. Lee**[1], **Mark Wallace**[4], **Koichi Masuda**[5], **Eric Y. Chang**[1,2], **Jiang Du**[1], **Ya-Jun Ma**[1]

[1]Department of Radiology, University of California San Diego, CA, United States

[2]Research Service, Veterans Affairs San Diego Healthcare System, CA, United States

[3]GE Healthcare, San Diego, CA, United States

[4]Department of Anesthesiology, University of California San Diego, CA, United States

[5]Department of Orthopedic Surgery, University of California San Diego, CA, United States

Abstract

Ultrashort echo time (UTE) sequences can image tissues with transverse T_2/T_2* relaxations too short to be efficiently observed on routine clinical MRI sequences, such as the vertebral body cartilaginous endplate (CEP). Here, we describe a 3D adiabatic inversion recovery-prepared fat-saturated ultrashort echo time (3D IR-FS-UTE) sequence to highlight the CEP of vertebral bodies in comparison to the intervertebral disc (IVD) and bone marrow fat (BF) at 3T. The IR-FS-UTE sequence used a 3D UTE sequence combined with an adiabatic IR preparation pulse centered in the middle of the water and fat peaks, while a fat saturation module was used to suppress the signal from fat. A slab-selective half pulse was used for signal excitation, and a 3D center-out cones trajectory was used for more efficient data sampling. The 3D IR-FS-UTE sequence was applied to an ex vivo human spine sample, as well as the spines of six healthy volunteers and of three patients with back pain. Bright continue lines representing signal from CEP were found in healthy IVDs. The measured contrast-to-noise ratio (CNR) was 18.5±4.9 between the CEP and BF, and 20.3±4.15 between the CEP and IVD for the six volunteers. Abnormal IVDs showed CEP discontinuity or irregularity in the sample and patients' studies. In conclusion, the proposed 3D IR-FS-UTE sequence is feasible for imaging of the vertebral body's CEP in vivo with high contrast.

Keywords

Cartilaginous Endplate; Adiabatic Inversion Recovery; Ultrashort Echo Time

Corresponding author: Ya-Jun Ma, Ph.D., yam013@ucsd.edu, Department of Radiology, University of California, San Diego, 9452 Medical Center Drive, La Jolla, CA 92037, Phone: (858) 246-2229.

Declaration of Competing Interest

The authors have no conflicts of interest to declare.

1. Introduction

Low back pain is the most common cause of disability in all ages and both sexes (1), presenting with high incidence and high recurrence rates (2). A multifactorial problem, low back pain may be associated with degenerative disc disease, vertebral body fractures, spondylolysis, spondylolisthesis, facet joint disorders, and instability (3). The cartilaginous endplate (CEP), a thin layer of hyaline cartilage between the vertebral body and the intervertebral disc (IVD), plays an important role in the transport of nutrients from blood vessels to disc cells (4). It is also associated with the transmission of mechanical loading between the IVD and the vertebral body, helping in the physiologic spine biomechanics (5). As the body ages, CEP becomes thinner, followed by mineralization and ossification (6). Atherosclerosis and narrowing of abdominal blood vessels contribute further to disturbances in nutrient transport through the CEP, and consequently, to degenerative changes in the IVD (7, 8). In addition, spine instability or vertebral body fractures that tend to affect the CEP can disrupt normal spine biomechanics, further exacerbating IVD degeneration (9).

For qualitative evaluation of IVD degeneration, available imaging techniques currently rely mostly on T_1- and T_2-weighted MRI sequences (10), which are not very efficient in detecting the CEP due to its short transverse relaxation times (T_2/T_2*) and rapid signal decay. Paravertebral muscles and bone marrow fat (BF) signal further complicate independent evaluation of the CEP in conventional MRI, limiting the ability to better understand the relationship between CEP abnormalities and IVD degeneration. There is clearly need for a better MRI sequence that individually detects the CEP with high resolution and high contrast, and that can be used to clinically evaluate the involvement of the CEP in IVD degeneration.

Ultrashort echo time (UTE) MRI sequences can overcome this limitation and are capable of imaging tissues with short T_2s (less than 1 ms) (11, 12). Different UTE techniques exist including those which use dual-echo subtraction (13), and those which apply adiabatic inversion pulses to suppress signals from tissues with long T_2, so as to highlight only the short T_2 tissues (14, 15). Dual-echo subtraction sequences have a low contrast-to-noise ratio (CNRs) between short T_2 tissues and BF (16, 17), due to the latter's high proton density and relatively short T_2* (18). UTE sequences that use adiabatic inversion pulses can produce higher contrast between tissues with short and long T_2s (14, 15, 19, 20). Furthermore, 3D adiabatic inversion recovery (IR) prepared UTE sequences allow volumetric data acquisition, which further reduces partial volume artifacts, making them potentially better suited for the evaluation of the CEP, a thin layer of hyaline cartilage. To the best of our knowledge, no IR-based 3D UTE sequences have been investigated for high contrast volumetric imaging of the CEP.

In this study, we report a 3D adiabatic inversion recovery prepared fat-saturated ultrashort echo time (3D IR-FS-UTE) MRI sequence to highlight the CEP region in relation to the IVD and adjacent BF. We expect this 3D IR-FS-UTE sequence can image the CEP in vivo with high resolution and high contrast.

2. Methods

2.1 MR Acquisition and Contrast Mechanism

The institutional review board approved this study. The 3D IR-FS-UTE sequence was implemented on a 3 T MR750 scanner (GE Healthcare Technologies, Milwaukee, WI, USA). An eight-channel knee coil was used for both RF transmission and signal reception in the ex vivo study, while a four-channel phased array spine coil was used for signal reception in the in vivo study.

The 3D IR-FS-UTE acquisition method and the contrast mechanism to highlight CEP signal are presented in Figure 1. The 3D IR-FS-UTE sequence uses an adiabatic inversion pulse (hyperbolic secant type 1 design, duration = 8.64 ms, bandwidth = 1.15 kHz) to invert the longitudinal magnetizations of IVD tissues (Figure 1A). The inversion pulse is centered at the frequency in the middle of the water and fat peak at 3T (i.e., −220 Hz) to robustly invert both water and fat longitudinal magnetizations (less sensitive to the B0 inhomogeneity). With proper selection of the inversion recovery time (TI), IR-type sequences can achieve a strong T_1 contrast. As reported by Moon SM et al. (21), CEP has a much shorter T_1 retaliation than both AF and NP. Thus, after an appropriately chosen TI — adjusted to null signals from long T_1 tissues (for instance, NP) — the 3D UTE data acquisition starts to selectively detect high signals from tissues with short T_1, in this case, the CEP. The current IR preparation cannot fully suppress the fat signals due to the much shorter T_1 relaxation of fat (thus a shorter TI needed for signal nulling) in contrast to the other long T_2 tissues such as the NP. To further suppress the fat signals, a widely used FatSat module is used before data acquisition to improve the contrast between CEP and fat. To speed up data acquisition, a train of spokes is used after each IR-FS preparation. A slab selective half pulse (Shinnar–Le Roux (SLR) design, duration = 1132 μs and bandwidth = 16 kHz) with variable-rate selective excitation (VERSE) design is used for signal excitation in each UTE acquisition spoke (Figure 1B) (22), and a 3D center-out cones trajectory (Figure 1C) is used to reduce sampling time with a TE of 32 μs (23, 24).

2.2 Ex Vivo Study of Spines Samples

Two cadaveric spine samples were obtained from a 68-year-old female donor and a 61-year-old male donor and scanned immediately after harvesting. The thoracolumbar junction was chosen due to the high prevalence of vertebral body fractures and degenerative changes in this region.

To investigate T_1 variations among all the tissue components in the IVD, including the CEP, NP and AF, T_1 relaxations were measured first with the 3D UTE actual flip angle and variable flip angle (UTE-AFI-VFA) method (25), followed by the clinical sequences T_1-weighted fast spin-echo (T_1w-FSE) (TR/TE = 815/6.7 ms) and T_2-weighted FSE (T_2w-FSE) (TR/TE = 3046/68.5 ms), as well as the proposed 3D IR-FS-UTE (TR/TI = 1200/600 ms) sequence. Following MR scans, a micro-computed tomography (μCT) scan was performed on samples to determine whether there were bone fractures that may have damaged the CEP structure. Study images were compared to previously acquired in vivo CT images from the same donor to assess any postmortem changes in the vertebral body bone morphology.

Detailed image parameters are listed in Table 1. The TI of the IR-FS-UTE sequence was determined experimentally to get a high CEP contrast and an oversampling factor of 2 was used to improve the image signal to noise ratio. Following MR and μCT imaging, the spine sample was fixed and sliced for histology.

2.3 Histology

Full-width spine segments were initially fixed for 2 days in 3.7% formaldehyde at room temperature, then manually sawed into 4 mm-wide sagittal sections containing target regions before one day of additional fixation. Pieces were decalcified with 10% disodium EDTA at pH7 at room temperature for 3 weeks, dehydrated, and embedded in paraffin. Five-micron paraffin sections were stained for glycosaminoglycans (GAGs) with Safranin-O and counterstained with Fast Green. Transmitted light images using a 2.5X objective were taken using an Olympus AH-2 microscope.

2.4 In Vivo Spine Study in Healthy Volunteers and Patients with Back Pain

We performed T_1w-FSE (TR/TE = 750/8.3 ms), T_2w-FSE (TR/TE = 5126/102 ms), and IR-FS-UTE (TR/TI = 1200/600 ms) MRI sequences on the cervical spine of one healthy female volunteer, on the lumbar spines of five healthy volunteers (aged 28 to 39 years old, three females, two males), and on the lumbar spines of three patients with low back pain (aged 42 to 72 years old, three males). We also compared the MR images and previous CT images from one of the symptomatic participants (72 years old male). Written informed consent was obtained from the volunteers and patients before the imaging examinations. Detailed imaging parameters are listed in Table 1.

2.5 Image Analysis

The non-linear fitting for IVD T_1 measurement was performed in Matlab R2018b (The MathWorks Inc., Natick, MA, USA) (23). All other imaging analyses were performed using Radiant Dicom Viewer version 2020.2.3 (Medixant, Poznan, Poland). CNR between the CEP and BF ($CNR_{CEP\text{-}BF}$) and between the CEP and IVDs ($CNR_{CEP\text{-}IVD}$) was calculated as the mean differences in signal between those tissues divided by the background noise. The regions of interest (ROIs) were drawn by one fellowship-trained musculoskeletal radiologist with eight years of experience. The noise was calculated as the standard deviation (SD) of the signal inside an ROI placed in an artifact-free background region. Mean and standard deviation were calculated.

3. Results

The cadaveric spine sample study showed higher signal differences between the CEP, IVD and AF with a higher FA. Figure 2 shows the T_1 measurement results of an IVD from a cadaveric spine sample. When the flip angle is lower than 8°, all contrasts among CEP, AF, and NP are low. The tissue contrast begins to improve when the flip angle is higher than 10°. When the flip angle reaches 20° only minor improvements of contrast is observed afterwards. The 3D UTE-AFI-VFA method showed a much lower T_1 for the CEP, compared to the AF and the NP.

As seen in Supplemental Figure 1, a high CEP contrast can be achieved by the 3D IR-FS-UTE sequence with a wide range of TIs for a fixed TR. This demonstrates the robustness of the proposed 3D IR-FS-UTE sequence (not sensitive to the TI selection) for high contrast CEP imaging. Supplemental Table 1 summarizes the measured CNRs between CEP and NP and between CEP and AF where it can be found that the best balance reached with TI was around 600 ms. For TI = 600 ms, the CNR calculated between CEP and NP was 84.6±17.7, and between CEP and AF was 79.6±5.7.

The cadaveric spine sample imaging study is an example that the CEP region cannot be visualized on the clinical sequences due to its short T_2/T_2^* (Figure 3A and B) but is clearly visualized on the 3D IR-FS-UTE sequence with high contrast in comparison to the IVD and vertebral body BF (Figure 3C and D). A compression fracture in L1 can be seen in this specific specimen (Figure 4 A–G). The in vivo CT and the μCT helped to confirm that the bright lines seen on the 3D IR-FS-UTE sequence are located adjacent to the vertebral endplates, representing the CEP. A subtle CEP abnormality is seen only on the 3D IR-FS-UTE sequence due to its high signal and high contrast with the surrounding structures. The histologic study later detected a CEP fracture with NP herniation in the same location (Figure 4E and G).

A healthy volunteer study (29-year-old female) showed the lumbar CEP which is invisible on the clinical T_1w- and T_2w-FSE MRI sequences but highlighted on the 3D IR-FS-UTE sequence (Figure 5). In addition, high contrast images of the longitudinal ligaments are also obtained on the 3D IR-FS-UTE sequence (Figure 5C and D) because of the short T_2 property of ligaments.

Figure 6 shows the high-resolution cervical spine images obtained with the proposed sequence in a healthy volunteer (28-year-old female) where the CEP is highlighted even in the small vertebral bodies, in contrast to the T_1w- and T_2w-FSE MRI sequences where the CEP cannot be seen.

One volunteer (38-year-old male) showed a small incipient Schmorl’s node on one of the vertebral body’s endplate, with a preserved thin CEP within it, pointing out that early IVD degenerative changes may be better studied using the 3D IR-FS-UTE sequence (Figure 7A–C).

The mean CNRs between the CEP and BF, and between the CEP and IVD for all six volunteers were 18.5±4.9 and 20.3±4.15, respectively.

The in vivo study with symptomatic patients confirmed the capability of the 3D IR-FS-UTE sequence to image the CEP and show spine abnormalities with distinct examples of degenerative and traumatic changes such as acute Schmorl’s nodes (Figure 8A–C), bone spurs, CEP thinning (Figure 8C), vertebral body compression fractures with broken CEP (Figure 8D–G).

4. Discussion

In this study, we showed the feasibility of a 3D IR-FS-UTE sequence to image the CEP region in the spine with high contrast in two ex-vivo cadaveric samples, six healthy volunteers and three patients with spine abnormalities. The lower T_1 of the CEP (Figure 2) in comparison with those of the AF and NP allow for high contrast between those structures when using the T_1-weighted 3D IR-FS-UTE sequence. The FatSat module is employed before data acquisition to improve the contrast between CEP and fat. The use of multiple-spoke sampling after each IR-FS preparation allow for more time efficient MRI acquisition, reducing the total scan time for clinical use (14). The 3D volumetric UTE data acquisition is essential for robust evaluation of small structures like the CEP. Bright continue line representing signal from the CEP were found in healthy IVDs while abnormal IVDs showed CEP discontinuity or irregularity in the sample and patients' studies.

Imaging of the CEP with conventional MRI sequences is complicated by its small dimensions and relatively short T_2/T_2^* tissue properties, which makes it almost invisible and indiscernible from the surrounding bone and soft tissues (26). UTE sequences can image tissues with short T_2/T_2^* in the order of a few hundred microseconds, enough to highlight the CEP. Previous studies have used 2D UTE sequences based on dual-echo (for short and long T_2 tissues) and subtraction of the longer echo from the shorter echo images (13, 27). However, as the CEP is a small structure surrounded by long T_2 tissues there are signals remaining from those tissues, leading to reduced image contrast for the CEP. Furthermore, eddy currents, off-resonance, and chemical shift artifacts are commonly present and lead to image blurring, adding to the low CNR, and complicating its clinical use (28). Other techniques such as utilizing the inversed contrast of the proton-density weighted FSE sequence was used to highlight the dark CEP (29). The healthy CEP displayed as a continuous white band while some abnormal CEPs show damage in the inversed contrast images. However, this technique cannot detect the CEP signal itself but assumes the bright signals in the signal inversed images are from CEP, which may be problematic in some conditions, such as vertebral body endplate fractures. In contrast, the combination of an adiabatic IR pulse and a FatSat module in our proposed 3D IR-FS-UTE sequence resulted in a real signal detection of CEP with high resolution and high contrast. As demonstrated in the T_1 measurements using the UTE-AFI-VTR technique, the CEP, and the BF both have relatively short T_1s, which made it possible to highlight the CEP with a T_1-weighted UTE sequence, verifying the rationality of the proposed 3D IR-FS-UTE sequence to use an IR preparation to create an effective T_1 contrast. However, if only the adiabatic IR pulse is used, there is a natural low contrast between the CEP and the BF, and the FatSat module adds significant contrast as it suppresses the signal from BF.

The IR-FS-UTE sequence is a highly T_1-weighted sequence which has the potential to replace the currently available clinical T_1w-FSE sequence. Compared with the T_1w-FSE sequence, IR-FS-UTE has the extra advantage of high CEP contrast. This in vivo study of healthy volunteers and patients showed how the proposed sequence might improve the accurate detection of early degenerative changes in the spine, including the evaluation of abnormalities such as irregularities, thinning, and complete discontinuity in the CEP, their presence or absence within Schmorl's nodes and fracture sites, and associated IVD changes

that cannot be routinely seen on T_1w- and T_2w-FSE MRI sequences. It may also be useful to distinguish early IVD degenerative changes, where the CEP is still present, from advanced degenerative changes, where the CEP may be thinned or completely disrupted. Patients with vertebral body fractures may also show dislocation of the CEP inside the fracture site, indicating acute fracture in a previously healthy IVD.

The high CNR obtained with our 3D IR-FS-UTE sequence potentially allows for the characterization of small CEP changes. Other potential applications are the evaluation of subtle abnormalities in the longitudinal ligaments, facet joints, and intervertebral foramina.

Our study has limitations. First, the small sample size did not allow us to examine the correlation between CEP abnormalities and IVD degenerative changes, although our initial objective was to demonstrate the feasibility of the newly proposed 3D IR-FS-UTE MRI sequence to image the CEP in the spine. Second, the commonly used FatSat module only allows fat saturation up to a certain limit in multi-spoke IR-FS-UTE imaging. The FatSat module reduces the fat suppression effectiveness when an increasing number of spokes is used to accelerate the imaging acquisition, thus creating a compromise between fat suppression and scan efficiency. This may be overcome by using a second adiabatic inversion pulse centered in the fat spectrum frequency to suppress fat signal, which will be studied in the future (15). Third, the FatSat module may potentially attenuate the CEP signal due to the direct and indirect (magnetization transfer effect) saturation. Again, a better fat suppression technique could be used to further improve the performance of CEP imaging in future. Fourth, the image resolution of the current IR-FS-UTE sequence was relatively low compared to the thickness of the CEP (i.e., approximately 0.6–1.0 mm), especially in the slice direction. There could be strong partial volume effect when imaging the curved regions. We expect to improve the imaging resolution without compromise of the scan time using k-space under sampling and advanced reconstruction techniques, such as compressed sensing and deep learning, in future studies (30, 31).

In conclusion, we demonstrated the feasibility of the proposed 3D IR-FS-UTE MRI sequence in imaging the CEP of the spine with high contrast, as well as its potential in diagnosing early IVD degenerative changes.

Supplementary Material

Refer to Web version on PubMed Central for supplementary material.

Acknowledgements

The authors acknowledge grant support from NIH (R01AR075825, R01AR062581, R01AR068987, R21AR075851), VA Clinical Science and Rehabilitation R&D Awards (I01CX001388 and I01RX002604), and GE Healthcare.

Data Availability

The data that support the findings of this study are available from the corresponding author upon reasonable request.

Abbreviations:

UTE	Ultrashort Echo Time
CEP	Cartilaginous Endplate
IR	Inversion Recovery
FS	Fat saturation
CNR	Contrast-to-Noise Ratio
IVD	Intervertebral Disc
BF	Bone Marrow Fat
NP	Nucleus Pulposus
AF	Anulus Fibrosus
FA	Flip Angle
VFA	Variable flip angle
ROI	Region of Interest
SLR	Shinnar-Le Roux
VERSE	Variable-rate selective excitation
GAG	Glycosaminoglycans

References

1. James SL, Abate D, Abate KH, Abay SM, Abbafati C, Abbasi N, et al. Global, regional, and national incidence, prevalence, and years lived with disability for 354 diseases and injuries for 195 countries and territories, 1990–2017: a systematic analysis for the Global Burden of Disease Study 2017. The Lancet. 2018;392(10159):1789–858.
2. Hoy D, Brooks P, Blyth F, Buchbinder R. The Epidemiology of low back pain. Best Practice & Research Clinical Rheumatology. 2010;24(6):769–81. doi: 10.1016/j.berh.2010.10.002. [PubMed: 21665125]
3. Deyo RA, Weinstein JN. Low back pain. N Engl J Med. 2001;344(5):363–70. Epub 2001/02/15. doi: 10.1056/nejm200102013440508. [PubMed: 11172169]
4. Whalen JL, Parke WW, Mazur JM, Stauffer ES. The intrinsic vasculature of developing vertebral end plates and its nutritive significance to the intervertebral discs. Journal of pediatric orthopedics. 1985;5(4):403–10. doi: 10.1097/01241398-198507000-00003. [PubMed: 4019751]
5. Brinckmann P, Frobin W, Hierholzer E, Horst M. Deformation of the vertebral end-plate under axial loading of the spine. Spine (Phila Pa 1976). 1983;8(8):851–6. Epub 1983/11/01. doi: 10.1097/00007632-198311000-00007. [PubMed: 6670020]
6. Bernick S, Cailliet R. Vertebral end-plate changes with aging of human vertebrae. Spine. 1982;7(2):97–102. doi: 10.1097/00007632-198203000-00002. [PubMed: 7089697]
7. Kauppila LI. Atherosclerosis and Disc Degeneration/Low-Back Pain – A Systematic Review. European Journal of Vascular and Endovascular Surgery. 2009;37(6):661–70. doi: 10.1016/j.ejvs.2009.02.006. [PubMed: 19328027]

8. Urban JPG, Smith S, Fairbank JCT. Nutrition of the Intervertebral Disc. Spine. 2004;29(23):2700–9. doi: 10.1097/01.brs.0000146499.97948.52. [PubMed: 15564919]

9. Inoue N, Espinoza Orías AA. Biomechanics of Intervertebral Disk Degeneration. Orthopedic Clinics of North America. 2011;42(4):487–99. doi: 10.1016/j.ocl.2011.07.001.

10. Pfirrmann CW, Metzdorf A, Zanetti M, Hodler J, Boos N. Magnetic resonance classification of lumbar intervertebral disc degeneration. Spine. 2001;26(17):1873–8. [PubMed: 11568697]

11. Chang EY, Du J, Chung CB. UTE imaging in the musculoskeletal system. Journal of magnetic resonance imaging. 2015;41(4):870–83. [PubMed: 25045018]

12. Fields AJ, Han M, Krug R, Lotz JC. Cartilaginous end plates: quantitative MR imaging with very short echo times—orientation dependence and correlation with biochemical composition. Radiology. 2015;274(2):482–9. [PubMed: 25302832]

13. Bae WC, Statum S, Zhang Z, Yamaguchi T, Wolfson T, Gamst AC, et al. Morphology of the cartilaginous endplates in human intervertebral disks with ultrashort echo time MR imaging. Radiology. 2013;266(2):564–74. [PubMed: 23192776]

14. Carl M, Bydder GM, Du J. UTE imaging with simultaneous water and fat signal suppression using a time-efficient multispoke inversion recovery pulse sequence. Magnetic resonance in medicine. 2016;76(2):577–82. [PubMed: 26309221]

15. Du J, Takahashi AM, Bae WC, Chung CB, Bydder GM. Dual inversion recovery, ultrashort echo time (DIR UTE) imaging: creating high contrast for short-T2 species. Magnetic Resonance in Medicine: An Official Journal of the International Society for Magnetic Resonance in Medicine. 2010;63(2):447–55.

16. Lee YH, Kim S, Song H-T, Kim I, Suh J-S. Weighted subtraction in 3D ultrashort echo time (UTE) imaging for visualization of short T2 tissues of the knee. Acta radiologica. 2014;55(4):454–61. [PubMed: 23934936]

17. Du J, Bydder M, Takahashi AM, Carl M, Chung CB, Bydder GM. Short T2 contrast with three-dimensional ultrashort echo time imaging. Magnetic resonance imaging. 2011;29(4):470–82. [PubMed: 21440400]

18. Kühn J-P, Hernando D, Meffert PJ, Reeder S, Hosten N, Laqua R, et al. Proton-density fat fraction and simultaneous R2* estimation as an MRI tool for assessment of osteoporosis. European radiology. 2013;23(12):3432–9. [PubMed: 23812246]

19. Larson PE, Conolly SM, Pauly JM, Nishimura DG. Using adiabatic inversion pulses for long-T2 suppression in ultrashort echo time (UTE) imaging. Magnetic Resonance in Medicine: An Official Journal of the International Society for Magnetic Resonance in Medicine. 2007;58(5):952–61.

20. Ma YJ, Jerban S, Carl M, Wan L, Guo T, Jang H, et al. Imaging of the region of the osteochondral junction (OCJ) using a 3D adiabatic inversion recovery prepared ultrashort echo time cones (3D IR-UTE-cones) sequence at 3 T. NMR in Biomedicine. 2019;32(5):e4080. [PubMed: 30794338]

21. Moon SM, Yoder JH, Wright AC, Smith LJ, Vresilovic EJ, Elliott DM. Evaluation of intervertebral disc cartilaginous endplate structure using magnetic resonance imaging. Eur Spine J. 2013;22(8):1820–8. Epub 2013/05/16. doi: 10.1007/s00586-013-2798-1. [PubMed: 23674162]

22. Hargreaves BA, Cunningham CH, Nishimura DG, Conolly SM. Variable-rate selective excitation for rapid MRI sequences. Magnetic Resonance in Medicine: An Official Journal of the International Society for Magnetic Resonance in Medicine. 2004;52(3):590–7.

23. Gurney PT, Hargreaves BA, Nishimura DG. Design and analysis of a practical 3D cones trajectory. Magnetic Resonance in Medicine: An Official Journal of the International Society for Magnetic Resonance in Medicine. 2006;55(3):575–82.

24. Wan L, Zhao W, Ma Y, Jerban S, Searleman AC, Carl M, et al. Fast quantitative 3D ultrashort echo time MRI of cortical bone using extended cones sampling. Magnetic resonance in medicine. 2019;82(1):225–36. [PubMed: 30821032]

25. Ma Y-J, Zhao W, Wan L, Guo T, Searleman A, Jang H, et al. Whole knee joint T1 values measured in vivo at 3T by combined 3D ultrashort echo time cones actual flip angle and variable flip angle methods. Magnetic Resonance in Medicine. 2019;81(3):1634–44. doi: 10.1002/mrm.27510. [PubMed: 30443925]

26. Kakitsubata Y, Theodorou DJ, Theodorou SJ, Tamura S, Nabeshima K, Trudell D, et al. Cartilaginous endplates of the spine: MRI with anatomic correlation in cadavers. J Comput

Assist Tomogr. 2002;26(6):933–40. Epub 2002/12/19. doi: 10.1097/00004728-200211000-00013. [PubMed: 12488738]

27. Gatehouse PD, He T, Hughes SP, Bydder GM. MR imaging of degenerative disc disease in the lumbar spine with ultrashort TE pulse sequences. Magma. 2004;16(4):160–6. Epub 2004/02/27. doi: 10.1007/s10334-003-0021-9. [PubMed: 14986145]
28. Wansapura JP, Daniel BL, Pauly J, Butts K. Temperature mapping of frozen tissue using eddy current compensated half excitation RF pulses. Magn Reson Med. 2001;46(5):985–92. Epub 2001/10/25. doi: 10.1002/mrm.1285. [PubMed: 11675651]
29. Mai R, Tan H, Zhao Y, Jia J, Liu W, Tian Y, et al. Diagnostic value and clinical significance of magnetic resonance imaging with the FS-PD-TSE sequence in diagnosing lumbar cartilaginous endplate failure. Eur Spine J. 2020;29(5):1121–30. Epub 2020/02/18. doi: 10.1007/s00586-020-06338-2. [PubMed: 32062760]
30. Lustig M, Donoho D, Pauly JM. Sparse MRI: The application of compressed sensing for rapid MR imaging. Magnetic Resonance in Medicine: An Official Journal of the International Society for Magnetic Resonance in Medicine. 2007;58(6):1182–95.
31. Wu Y, Ma Y, Liu J, Du J, Xing L. Self-attention convolutional neural network for improved MR image reconstruction. Information sciences. 2019;490:317–28. [PubMed: 32817993]

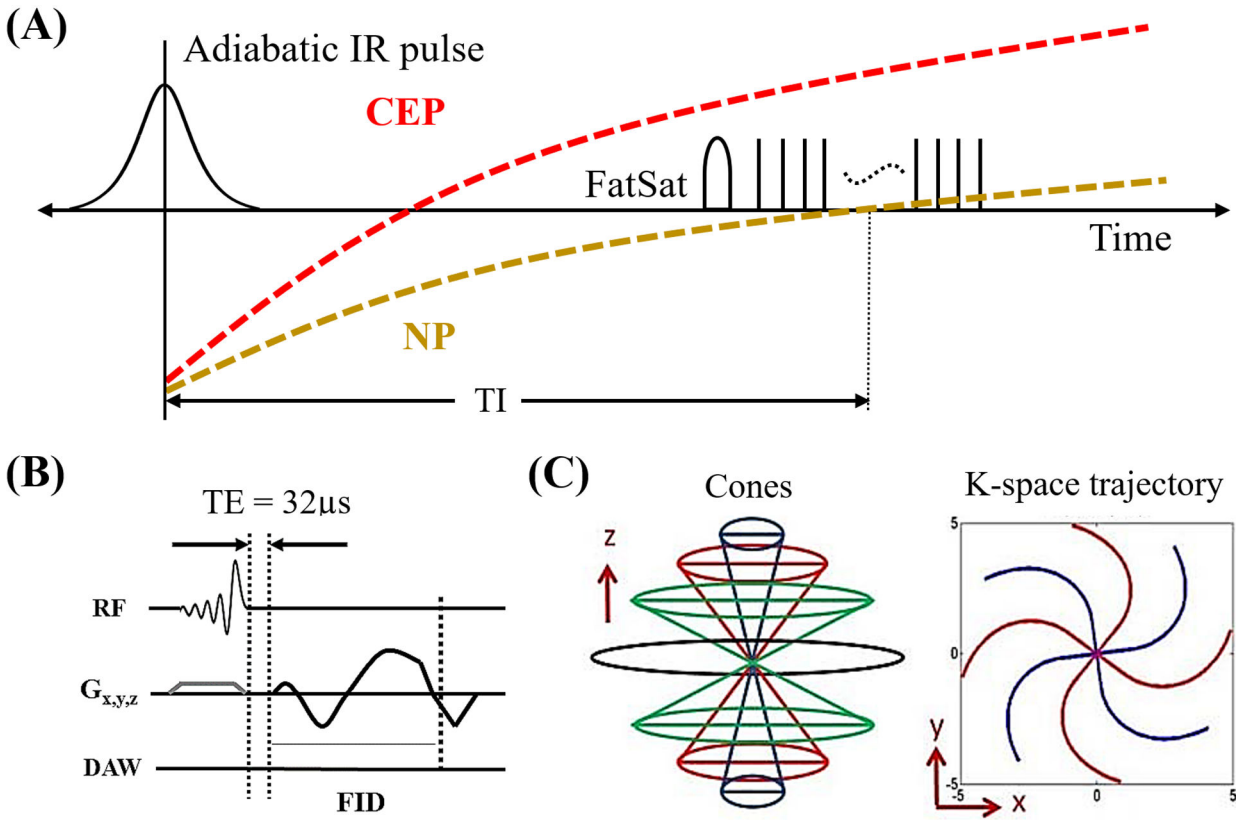

Fig 1.

3D IR-FS-UTE sequence diagram. The 3D IR-FS-UTE sequence employs an adiabatic IR pulse to invert IVD tissues, such as the NP (A). When TI is selected to suppress the NP, the CEP expresses high signal due to its short T_1 and fast M_z recovery. A FatSat module is used to further improve CEP contrast against BF. Multiple UTE spokes are sampled after each IR preparation to speed up data acquisition. Each UTE employs a half slab selective pulse with the VERSE design for signal excitation (B), followed by a Cones trajectory (C) to allow time-efficient sampling with TE 32 μs.

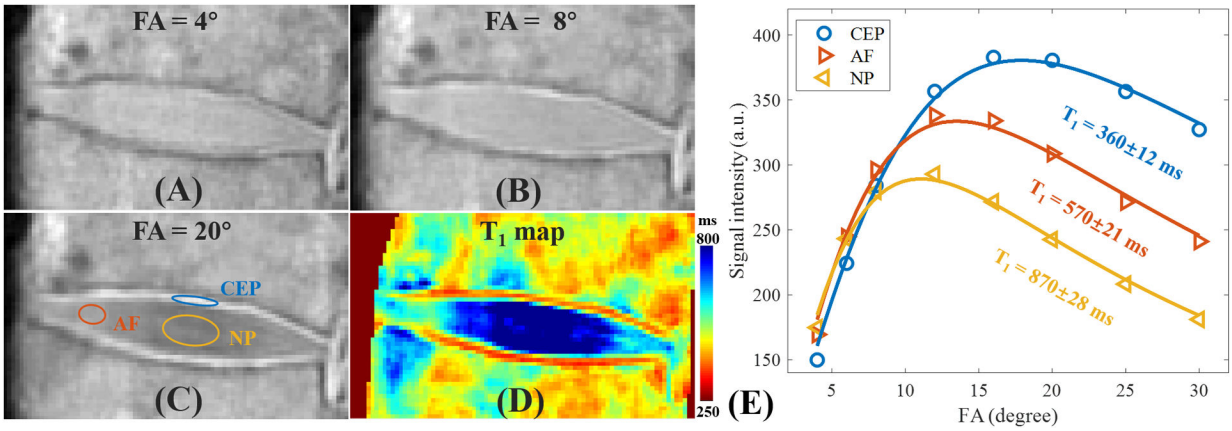

Fig 2.

T_1 measurement of the IVD from a spine sample (T9-T10, 61-year-old male donor). Panel A, B and C are the representative UTE-VFA images with flip angles of 4°, 8° and 20°, respectively. The generated T_1 map can be found in panel D. The fitting curves and corresponding T_1 values for the CEP (blue oval in panel C), AF (orange oval in panel C) and NP (yellow oval in panel C) are 360±12 ms, 570±21 ms, and 870±28 ms, respectively (E).

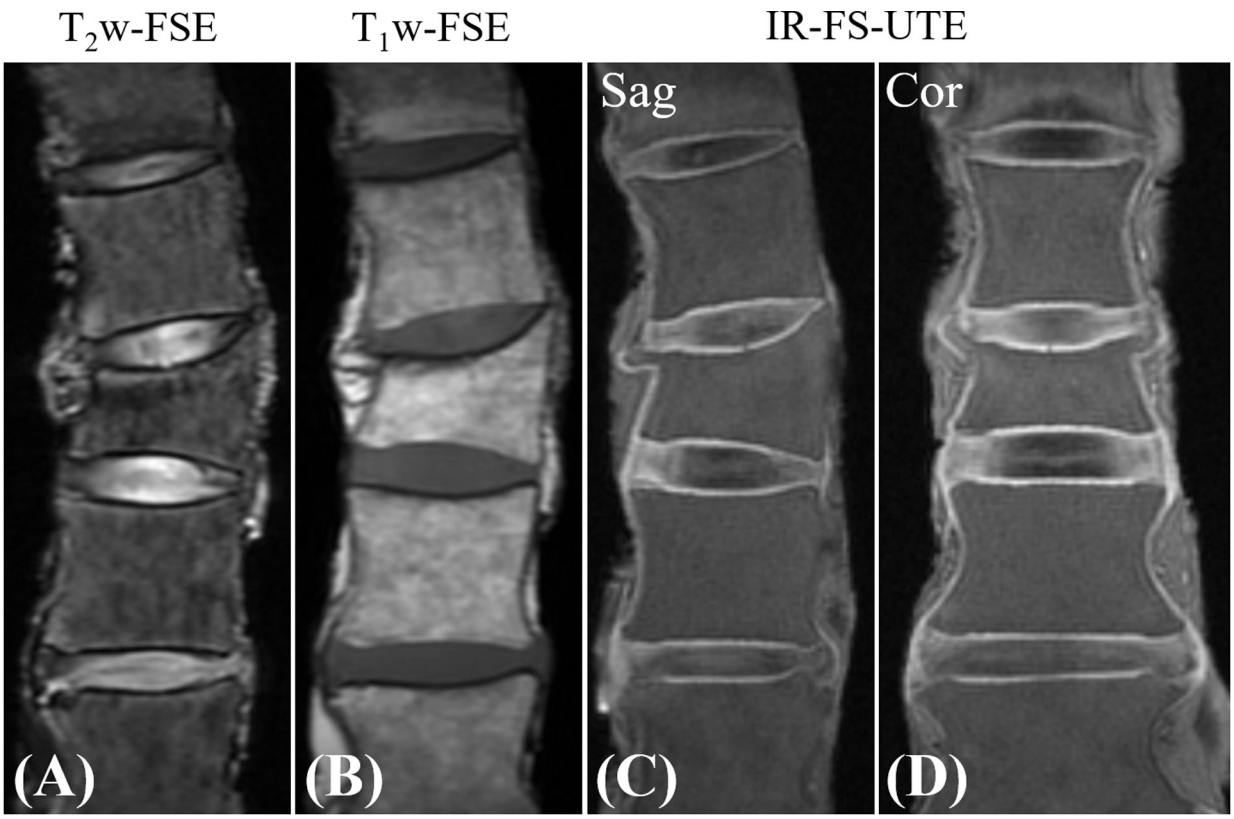

Fig 3.

T_2w-FS (A), T_1w-FSE (B), and IR-FS-UTE (sagittal: C, coronal: D) images from a spine sample (T11-L3, 68-year-old female donor). T10 and L4 were not shown due to the low signal intensity (close to the coil boundary). Note the compression fracture in L1.

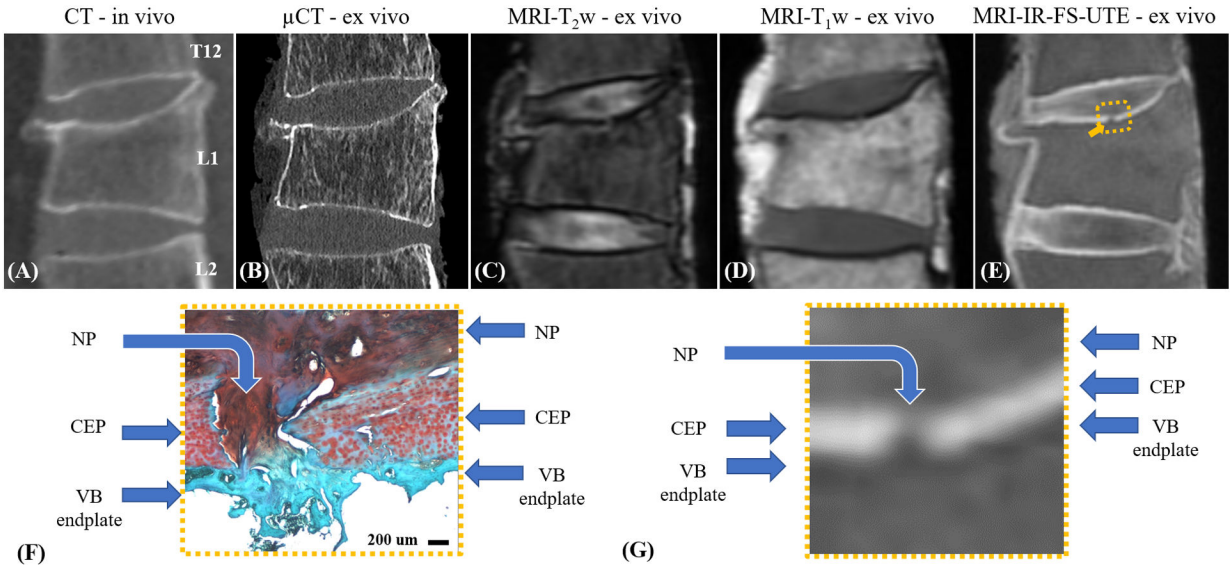

Fig 4.

Images of T12-L2 from in vivo CT (A) obtained prior to the patient's death as well as postmortem ex vivo μCT (B), clinical sagittal T_2w- and T_1w-FSE (C and D), and 3D IR-FS-UTE sequences (E). In addition to the compression fracture there is also a CEP fracture in the superior endplate of L1 with herniation of the NP through the focal defect as indicated on the IR-FS-UTE image (E) with a yellow arrow. This is further confirmed with histology (F). For better comparison with the histology image (F), the corresponding fracture region (yellow box) in IR-FS-UTE image (E) is zoomed in (G).

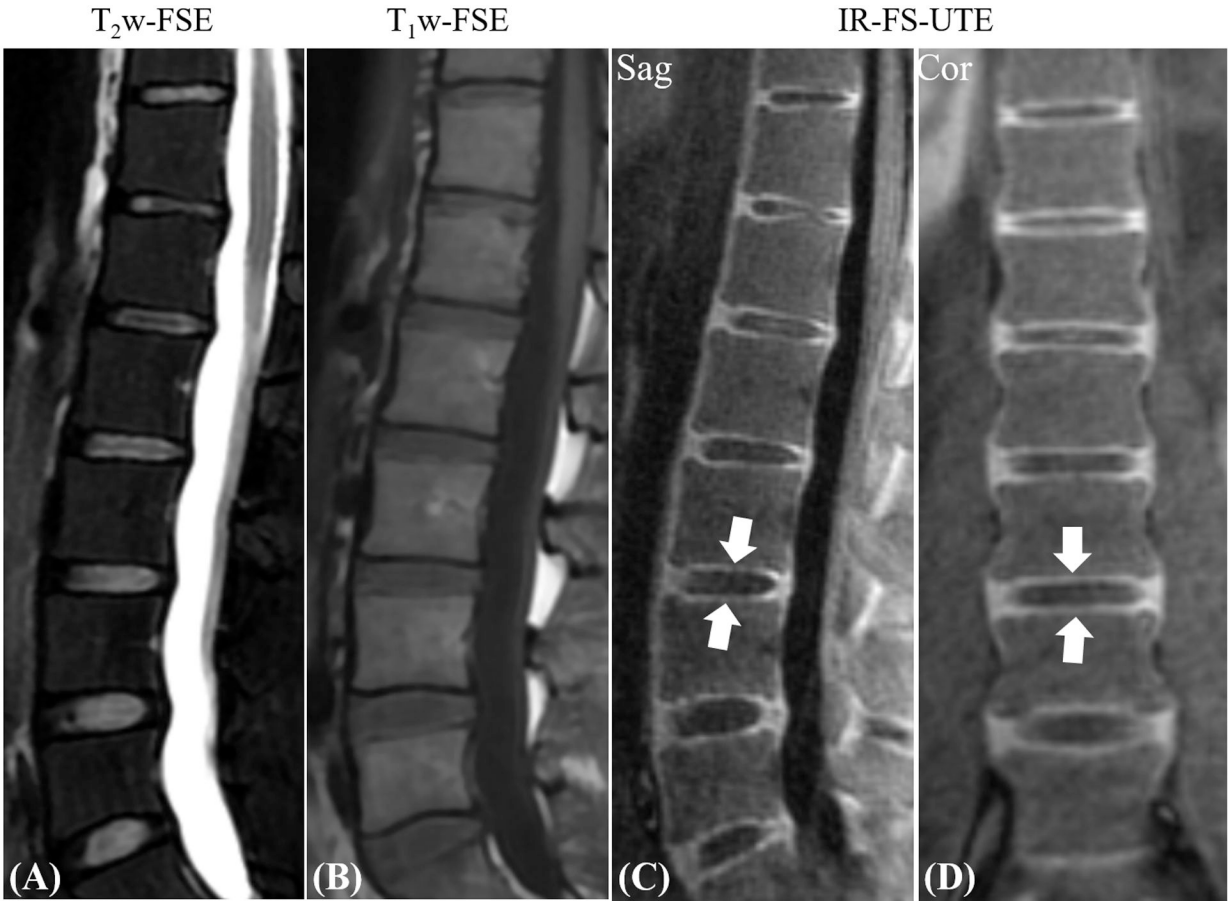

Fig 5.

Sagittal T_2w- and T_1w-FSE images (A and B), as well as sagittal and coronal 3D IR-FS-UTE images (C and D) from a 29-year-old female asymptomatic volunteer (T11-L5). The CEP is highlighted on both sagittal and coronal IR-FS-UTE images (arrows), while it is invisible on clinical sequences.

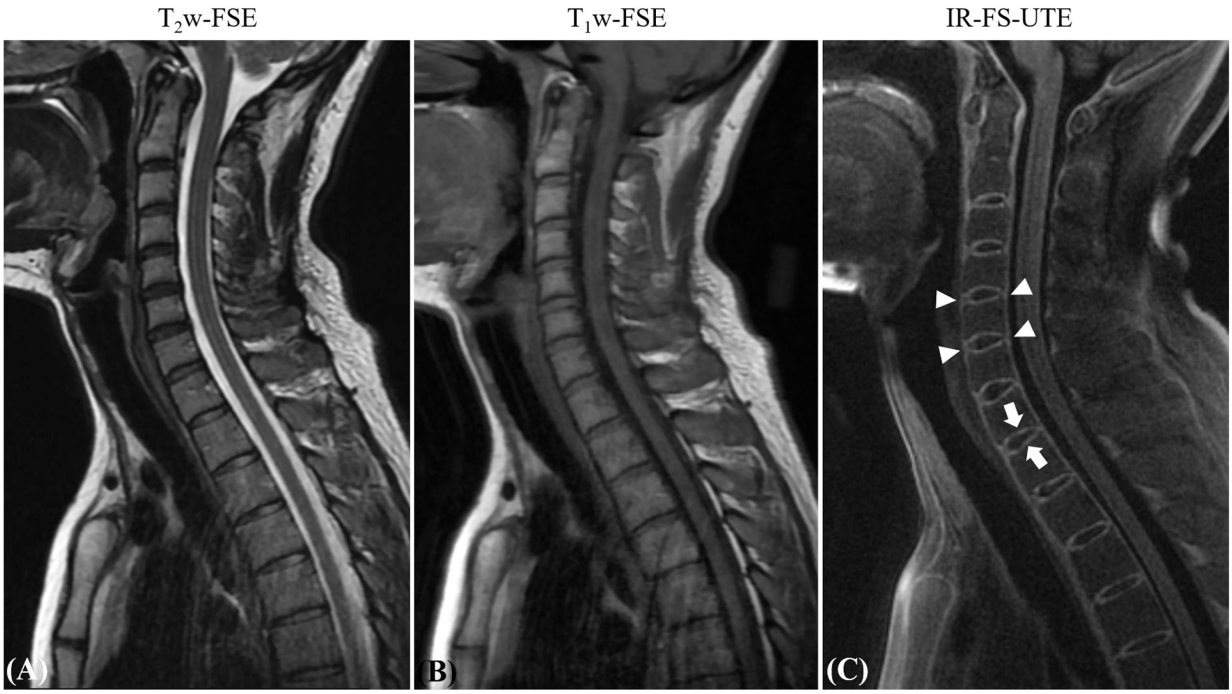

Fig 6.

Sagittal T_2w- and T_1w-FSE images (A and B) as well as sagittal 3D IR-FS-UTE images (C) from a 30-year-old female asymptomatic volunteer (C1-T6). The CEP is highlighted on the 3D IR-FS-UTE images (arrows in C) but cannot be seen on clinical sequences (A and B). Note also the anterior and posterior longitudinal ligaments highlighted on the 3D IR-FS-UTE sequence (arrowheads).

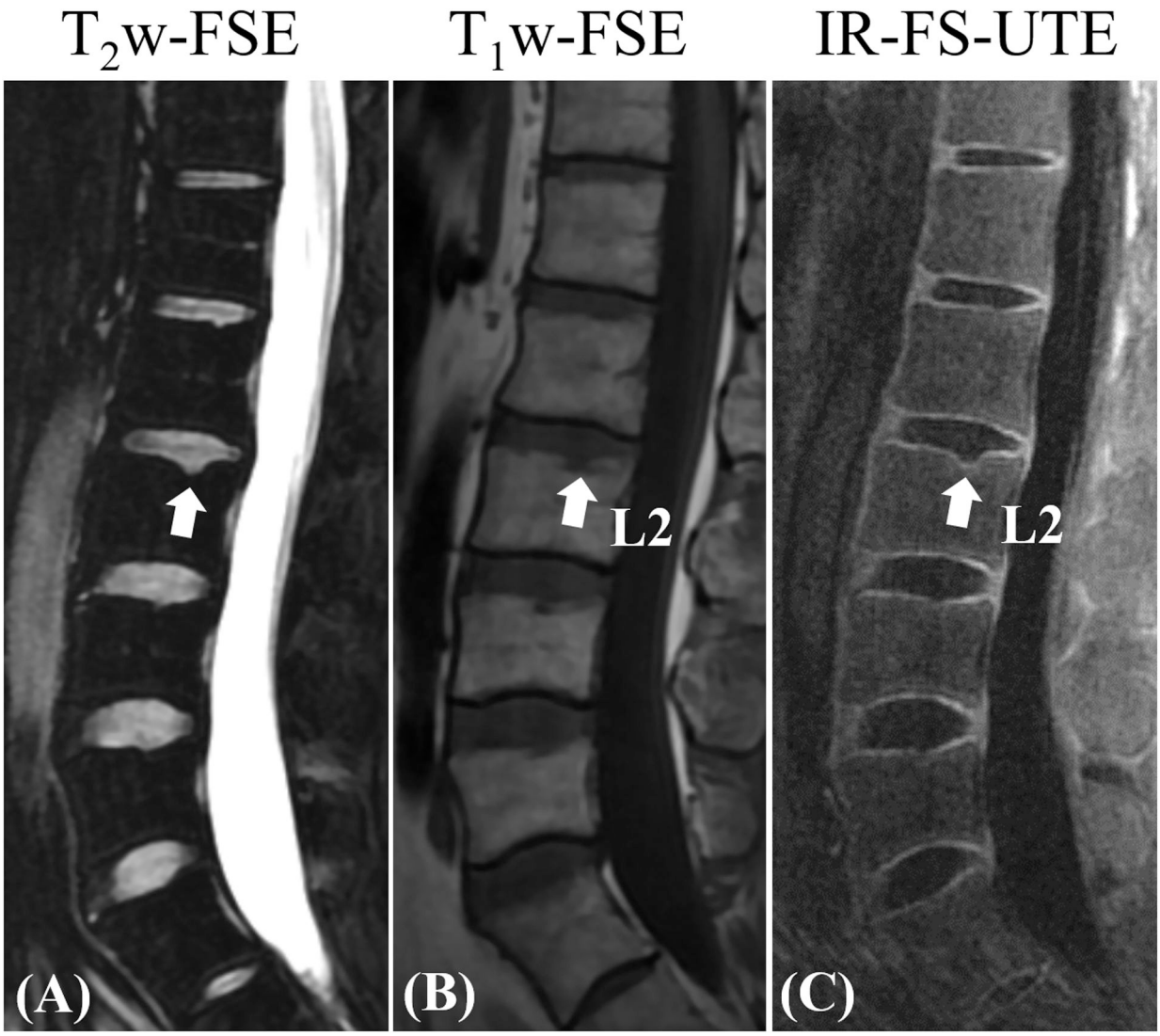

Fig 7.

Sagittal T_2w- and T_1w-FSE images (A and B) as well as sagittal 3D IR-FS-UTE images (C) from a 38-year-old male volunteer (T11-L5). The CEP is highlighted on the 3D IR-FS-UTE images (arrows in C) but cannot be seen on clinical sequences (A and B). Note the small and incipient Schmorl's node in the superior endplate of L2, with preserved CEP, that is only observed on the 3D IR-FS-UTE (arrows in A, B and C).

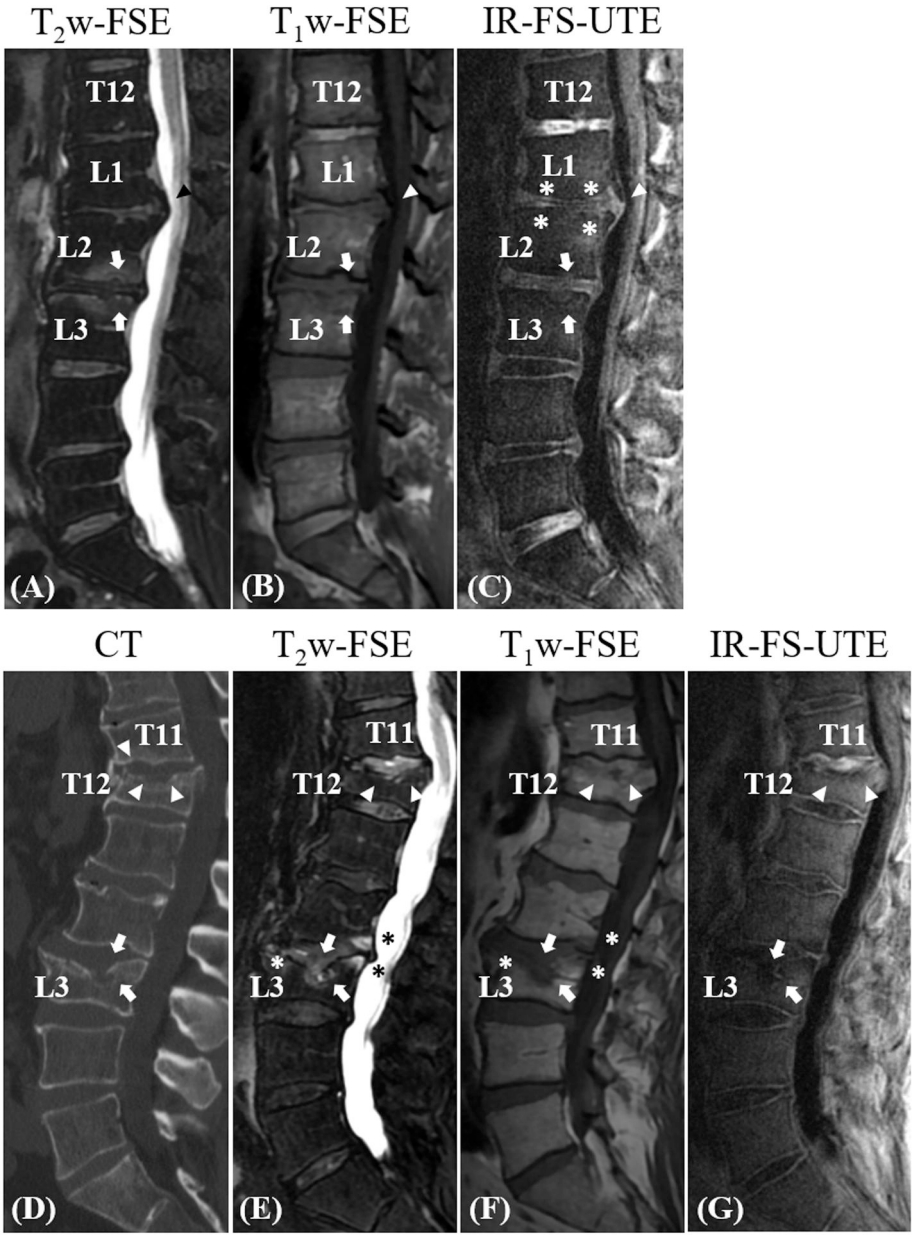

Fig 8.

Sagittal T_2w- and T_1w-FSE images (A and B) as well as sagittal 3D IR-FS-UTE images (C) from a 42-year-old male patient with low back pain (T12-S1). Schmorl's nodes and bone marrow edema are present in the L2 inferior endplate and L3 superior endplate (white arrows in A-C). Note the interruption in the CEP within the Schmorl nodes, only observed on the 3D IR-FS-UTE sequence (C). A posterior IVD bulge is seen between L1 and L2 (black arrowhead in A and white arrowheads in B and C); however, the posterior longitudinal ligament and a bone spur are also seen on the 3D IR-FS-UTE sequence (white arrowhead in C) and better highlighted compared to the T_2w-FS and T_1w-FSE sequences. Also note the disappearance of the CEP bright line from the vertebral endplates in L1-L2 (white asterisks in C), associated with IVD height loss and indicating advanced degenerative

changes. Sagittal reconstructed in vivo CT image (D), sagittal T_2w- and T_1w-FSE images (E and F) as well as sagittal 3D IR-FS-UTE images (G) from a 72-year-old male patient with low back pain (T10-S1). CT images show T12 and L3 upper endplate fractures and a small lower endplate fracture in T11 (white arrowheads and arrows, respectively in D). The corresponding clinical T_2w- and T_1w-FSE sequences (E and F) show areas of bone marrow edema especially in L2 and L3 (asterisks in E and F). The CEP can only be seen on the 3D IR-FS-UTE sequence (G) and it is discontinuous or broken in the areas of fracture (arrowheads and arrows in G).

Table 1

Sequence parameters for both ex vivo and in vivo spine studies.

	3D UTE-AFI-VTR	Clinical 2D T_2w-FSE	Clinical 2D T_1w-FSE	3D IR-FS-UTE
Ex vivo	FOV = 12×12×7.2 cm^3, Matrix = 300×300×36, BW = 125 kHz, AFI: (TR_1/TR_2 = 20/100 ms, FA = 45°), VTR (TR = 20 ms, FA = 4°, 6°, 8°, 12°, 16°, 20°, 25° and 30°), scan time = 1h 10 min	FOV = 24 × 24 cm^2, Matrix = 384 × 256, slice thickness = 3 mm TR = 3046 ms, TE = 68.5 ms, number of slices = 18, BW = 62.5 kHz, scan time = 3 min 10 sec	FOV = 24 × 24 cm^2, Matrix = 384 × 256, slice thickness = 3 mm TR = 815 ms, TE = 6.7 ms, number of slices = 18, BW = 62.5 kHz, scan time = 2 min 40 sec	FOV = 24×24×6.24 cm^3, Matrix = 320×320×52, TR/TI = 1200/600 ms, TE = 0.032 ms, FA = 10°, N_{sp} = 15, τ = 5.2 ms, BW = 250 kHz, oversampling factor = 2, scan time = 1 hour 22 min

	Clinical 2D T_2w-FSE	Clinical 2D T_1w-FSE	3D IR-FS-UTE
In vivo	FOV = 34 × 34 cm^2, Matrix = 360 × 270, slice thickness = 3.5 mm TR = 5126 ms, TE = 102 ms, number of slices = 14, BW = 70.3 kHz, scan time = 2 min 15 sec	FOV = 34 × 34 cm^2, Matrix = 360 × 270, slice thickness = 3.5 mm TR = 750 ms, TE = 8.3 ms, number of slices = 14, BW = 70.3 kHz, scan time = 1 min 40 sec	FOV = 28×28×4.32 cm^3, Matrix = 320×320×12, TR/TI = 1200/600 ms, TE = 0.032 ms, FA = 10°, N_{sp} = 17, τ = 5.2 ms, BW = 125 kHz, scan time = 9 min 52 sec

FOV: field-of-view; TR: repetition time; TI: time of inversion recovery; TE: echo time; FA: flip angle; N_{SP}: number of spokes per TR; τ: time between spokes; FA: flip angle; BW: bandwidth IR: inversion recovery; FS: fat saturation.

The slice number of the IR-FS-UTE sequence is adjustable according to the IVD width in the left- right direction.